UNIVERSITÀ DEGLI STUDI DI TORINO

Synthesis of α-Quartz with Controlled Properties for the Investigation of the Molecular Determinants in Silica Toxicology

Linda Pastero[1,3,4,5*], *Francesco Turci* [2,3,4], *Riccardo Leinardi* [2,4], *Cristina Pavan* [2,4], *Marco Monopoli* [6]

[1] Department of Earth Sciences, Via Valperga Caluso, 35, 10125 Torino, Italy
[2] Department of Chemistry, University of Torino, Via Pietro Giuria 7, Torino, Italy
[3] NIS Interdepartmental Center for Nanostructured Interfaces and Surfaces, Via Pietro Giuria 7, Torino, Italy
[4] G. Scansetti Interdepartmental Centre for Studies on Asbestos and Other Toxic Particulates, Via Pietro Giuria 7, Torino, Italy
[5] CrisDi Interdepartmental Center for Crystallography, Via Pietro Giuria 7, Torino, Italy
[6] Centre for BioNano Interactions, School of Chemistry and Chemical Biology, University College Dublin, Dublin 4, Ireland

** Corresponding Author*
e-mail: linda.pastero@unito.it
Dipartimento di Scienze della Terra, Università degli Studi di Torino
Via Valperga Caluso 35 – 10125 Torino (Italy)

Keywords: crystal growth, hydrothermal synthesis, silica, α-quartz, sol–gel processes

Abstract

Many experimental studies about the harmful effects of crystalline silica on human health are present in literature. However, the relationship between toxicological properties and surface functionalities of quartz are not yet fully explained because of the large intrinsic variability of natural samples. Specific surface properties are related to the surface structure: this implies that a reliable constraint on the crystal growth morphologies is necessary in order to control the behavior variability. With a view to understanding this relationship, a consistent, clean and easy way to crystallize quartz is proposed. In this paper α-quartz crystals with controlled morphology and properties were prepared by an unusual and accurate approach under mild hydrothermal conditions (200°C, autogenic pressure) starting from silica gels prepared with different polymerizing agents. Gels and synthetic crystals were characterized using a wide range of experimental techniques: elemental analysis by ICP-OES, X-Ray Powder Diffraction and Rietveld analysis, SEM and HR-TEM microscopies, BET surface analysis, Differential Centrifugal Sedimentation, and FT-IR spectroscopy.

Results are discussed in the light of the crystal growth mechanisms involved, paying attention to the role of this synthetic quartz in defining the molecular determinants in silica toxicology.

1. Introduction

During the last 150 years, the interest about synthesis and crystal growth of α-quartz encompassed naturalistic, industrial, and toxicological researches. In these fields, an increasing attention has been devoted to tailoring quartz crystal size investigating surface properties, and understanding the interaction relation between crystal surface and biomolecules at the molecular level.[1,2,3,4,5]

In this context, the synthesis of amorphous silica and crystalline SiO_2, with controlled properties has become a research frontier in the investigation of the molecular mechanism in silica toxicology. [6]

Crystalline silica is a well-known carcinogenic agent, and its inflammogenic potential has been often correlated to the occurrence of some specific surface properties.[7,8, 9,10,4, 6] A large body of scientific literature exits on the mechanisms that elicit quartz-induced detrimental effects on human health.[11,12] Nevertheless, previous attempts to draw structure-activity relationship (SAR) between quartz physico-chemical properties, including size, surface charge and surface functionality, have not yet provided a definitive picture, mainly because of the large intrinsic variability of natural quartz. A bottom-up synthetic approach has been largely exploited to systematically investigate the physico-chemical determinants of the interaction of amorphous silica with biological environment, including protein, membrane, and cell.[13, 14,15, 16] Adapting this approach to crystalline silica, well-formed and surface-tailored synthetic crystals could be exploited to investigate the molecular nature of the interaction between quartz and living matter.

Many pioneering papers dealing with the hydrothermal synthesis of α-quartz from pure silica aqueous solutions or from amorphous silica in the presence of impurities (typically alkali halides and alkali hydroxides) were published since the second part of the 19th century. Inevitably, the negligible solubility of silica in water in standard conditions requires high pressure and temperature to completely dissolve the supply material and the quenching of the solution to induce nucleation of quartz commonly yields some amorphous unreacted material to remain at the end of the experiment.[17] Moreover size and properties of the synthetic crystals are difficult to control.

Li and coworkers obtained spherulitic growth of quartz aggregates starting from a silica gel obtained by mixing a silica solution with hydrochloric acid until polymerization was reached. [18] Quartz crystals were characterized following the procedure proposed by Zhdanov but neither control over crystallite size and surface properties was achieved, nor explanations about the mechanism of crystal growth from gel were proposed. [19]

In the present work, a similar unconventional sol/gel approach which employs Na-metasilicate solution (Na-MTS) polymerized using mineral acids has been followed. To keep the chemical complexity of the gel as low as possible, HNO_3 and H_2CO_3, were used as polymerizing agents. The advantage of using a gel during the crystallization of large crystals of sparingly soluble salts mainly resides in the low supersaturation reached into the porous medium reaction even in the presence of high concentrated solutions. This limits the number of nuclei reaching the critical size and decreases the crystal growth rate, allowing to control the surface reaction rate.[20, 21] Some of us showed that the growth of large crystals from slightly soluble salts can be successfully carried out in gel under pure diffusive regime.[22] Moreover, a gel minimizes the mechanical stress generated by the interactions among crystals, and between crystal and reactor wall coming to a

suitable way to mimic microgravity conditions, allowing to discriminate the effects of convection and diffusion during the crystal growth processes.[23]

Commonly, gel is assumed to be a chemically inert "glassy sponge", limiting the reaction rate and the effect of convection and gravity, disregarding the reactions between gel main constituents and counter ions, but, during growth of silicates, it may act as a semi-infinite reservoir [24–27] of highly reactive silica. Therefore, a systematic characterization of the gel properties was carried out by evaluating gel structure and performance in fluid transport and substrate effectiveness (ICP-OES, SEM). The crystal structure (XRPD and TEM), surface area (Kr-BET), crystal morphology (SEM and TEM), particle size distribution (DCS) and chemical proximity of surface silanols (FT-IR spectroscopy) of the synthesized α-quartz crystals were evaluated and compared to a pure natural quartz, previously used in many toxicological studies. Then, we succeeded in controlling, for the first time some crystal properties (size, surface quality, defects) by modulating gel composition and reaction condition. The mechanism for quartz formation supported by the proposed gel–induced crystal growth is also discussed.

2. Experimental

2.1. Materials and reagents

Silica gel was prepared from 25% w/w Na-MTS solution (sodium metasilicate pentahydrate, Aldrich). The gel was polymerized using two mineral acids: i) HNO_3, and ii) H_2CO_3 obtained by bubbling CO_2 into the Na-MTS solution until gel formation. The two gels are hereafter referred as NG and CG. Due to the weak acid dissociation constants of H_2CO_3 ($K_{a1} = 4.3 \cdot 10^{-7}$, $K_{a2} = 4.7 \cdot 10^{-11}$), the CG gel was stabilized at pH = ca. 8. A compatible pH range (between 7 and 8) was used with HNO_3 as polymerizing agent to ensure the highest consistency during growth. Growth runs of 12 to 168 hours were performed at 200 °C and autogenic pressure in

PFTE liner sealed into steel autoclaves. Ultrapure water was employed for all solutions. All other reagents were of analytical purity grade and were supplied by Sigma.

A pure quartz specimen from Madagascar largely employed in several toxicological studies was used as comparison in some experiments.

2.2. Inductively coupled plasma spectroscopy (ICP-OES)

Elemental analysis of Na-MTS quartz-forming gels was carried out to investigated partition and properties of the CG and NG gels. Moving solution inside the gels were extracted by spin dryer in order to evaluate their elemental compositions. Elemental analysis of free silicon and sodium inside these solutions was performed by ICP-OES (Thermo Jarrel Ash IRIS Advantage optical plasma spectrometer) under the following operating conditions: flush and analysis pump rate 2.22 ml/min, nebulizer pressure 23 psi, RF power 950 W.

Speciation into the sol/gel systems and saturation index calculations were performed using the PHREEQC program.[28]

2.3. XRPD and Rietveld analysis

Structural analysis of synthetic quartz crystals was carried out by X-ray powder diffraction (XRPD) using a PANalytical PW3040/60 X'Pert PRO MPD X-ray powder diffractometer. Crystal phases and crystal quality were identified and evaluated by Rietveld data analysis (cell deformation with respect to the NIST SRM 1878a standard and crystallite size) using the MAUD program (Materials Analysis Using Diffraction), a diffraction analysis program mainly based on the Rietveld method.[29, 30]

2.4. Electron microscopies (SEM and HR-TEM)

Sample morphology was investigated by Scanning Electron Microscopy (SEM), Cambridge S-360 and Hitachi S-4300 Field Emission Scanning Electron Microscope. Crystal samples were sonicated for 30 minutes in ultrapure water, dropped off on conductive stubs, and coated with

gold in order to prevent the electron beam from charging the sample. The operating conditions were: EHT 15 to 25 kV, WD 1 to 6 mm, probe current 100 pA.

To give evidence of the local structural lattice order of the outer shells surrounding the crystals and to inspect the defectiveness of the quartz samples High-resolution Transmission Electron Microscopy (JEOL 3010-UHR-TEM) equipped with a LaB6 filament operated at 300 kV, beam current 114 μA and equipped with a 2k x 2k pixels Gatan US1000 CCD camera was carried out. Elemental analysis was performed by Oxford INCA X-ray energy dispersive spectrometer (X-EDS) with a Pentafet Si(Li) detector. Quartz samples were dispersed in ultrapure water (MilliQ system, Millipore), sonicated for 20 minutes and a droplet was deposited on lacey carbon Cu grids.

2.5. BET surface analysis

Surface area of the quartz crystals was measured by means of the BET method based on Kr adsorption at 77 K (ASAP 2020 Micrometrics, Norcross, GA).

2.6. DCS (Differential Centrifugal Sedimentation)

The particle size distribution (PSD) of the synthetic and natural quartz samples has been determined by injecting ca. 100 μL of the sample suspended in phosphate buffer (PB, pH 7.4) in a CPS Disc Centrifuge (CPS Instruments, Europe) operated at 14k × g with a 6%-24% sucrose gradient in PB. Each experiment has been repeated at least twice. Size distribution data are plotted by relative weight %.

2.7. FT-IR Spectroscopy

For the FTIR measurements (Bruker IFS28; resolution = 2 cm-1; DTGS detector), the quartz samples, pressed into self-supporting pellets, were placed into a quartz IR cell equipped with KBr windows. Spectra were collected on pellets in air. Physisorbed molecular water was then removed at room temperature (RT) or at 400 °C by connecting the cell with the sample to a

conventional vacuum line (residual pressure = 1×10^{-6} Torr, 1 Torr =133.33 Pa) equipped with a liquid-N_2 cold-trap.

3. Results

3.1. Gel characterization

In a sol/gel crystallization experiment, the gel can be considered as a wet sponge with a mobile solution flowing within interconnected cavities with variable pore size.

A thorough characterization was performed on both HNO_3 polymerized gel (NG) and CO_2 polymerized gel (CG). To characterize the volume and composition of the solution that flow through the cavities and to understand the growth mechanisms determining different crystal quality, NG and CG gels were prepared, then they were aged at room temperature or heated at the crystallization temperature (200 °C) and autogenic pressure, so simulating a growth experiment, for 6 hours. Such a short reaction time is not sufficient to obtain detectable quartz crystals, but, when the temperature is raised, the convective regime is enhanced and the solution entrapped into the “glassy sponge” is forced to flow. Consequently the gel structure changes and the transport regime moves from nearly pure diffusive to plainly convective: the gel role turns from sponge to nourishing reservoir. In order to evaluate the increase of the convective component of the flow, the aged/heated gels were centrifuged and the flowing solution was separated from the solid fraction. For each portion of gel, the percentage of extractable solution with respect to the total gel weight was measured. The Na and Si concentration in the two flowing solutions was measured by ICP-OES and compared with those in the Na-MTS starting solutions.

In this way, the concentration of the circulating sodium and silica was evaluated for each gel to qualitatively estimate the transport and supersaturation conditions inside each reactor during quartz growth and to explain the quality of the crystals.

Elemental data are reported in **Table 1**.

Table 1. Percentages of circulating ions in solution and of total flowing solution in a Na-MTS gel polymerized with nitric acid (NG) or CO_2 bubbling into the metasilicate solution (CG). Percentages are calculated with respect to the starting total concentration in the gels.

	RT gel		200 °C gel	
	NG	**CG**	**NG**	**CG**
%Na^+	45	14	99	97
%Si^{4+}	5	1	5	13
pH	9.9	11.5	11.7	11.7
% w/w flowing solution	35	58	83	99

The percentage of extractable solution in CG reaches the striking value of 99% at 200°C, with respect to the 83% in the NG case. This means that, in the CG case, the solution is free to flow supplying silica and mitigating supersaturation gradients during crystal growth. On the contrary, in the NG case, the volume of flowing solution is smaller and the supply of silica to the growing crystals is lower.

The high pH values in all cases fit with the presence of dissolved silica.

In the NG case, ageing the sample at 200°C, entails an apparent increase in sodium availability and a constant free silicon percentage, but considering the dilution due to the increase of the moving solution from 35% to 83%, the free sodium percentage becomes constant and the free silicon decreases. On the contrary, in CG case, heating the gel brings to an increase for both sodium and silicon.

Speciation calculations performed using the PHREEQC software confirm the presence of host phases with concentration in solution lower than their saturation values both at room temperature and at the growth temperature of quartz: nitratine ($NaNO_3$) in the NG gel and trona ($Na_3H(CO_3)_2 \cdot 2H_2O$), natron ($Na_2CO_3 \cdot 10H_2O$), and thermonatrite ($Na_2CO_3 \cdot H_2O$) in CG case. The occurrence of some among these guest phases precipitated from the dehydrated gel was confirmed by XRPD giving evidence of nitratine in NG and trona in CG.

The gel matrix before quartz crystallization has a sponge-like behavior, as shown in **Figure1**a). The early stages of quartz crystallization are shown in Figure1.b) to f). The presence of a substrate favoring the heterogeneous nucleation (the inner and outer walls of the bubbles) lowers the activation energy for nucleation of quartz that turns from 3D homogeneous nucleation in the volume to 2D heterogeneous nucleation on the substrate. This suggests that the gel works as substrate and hence induces the nucleation of quartz at lower supersaturation values than those required in growth from solution.

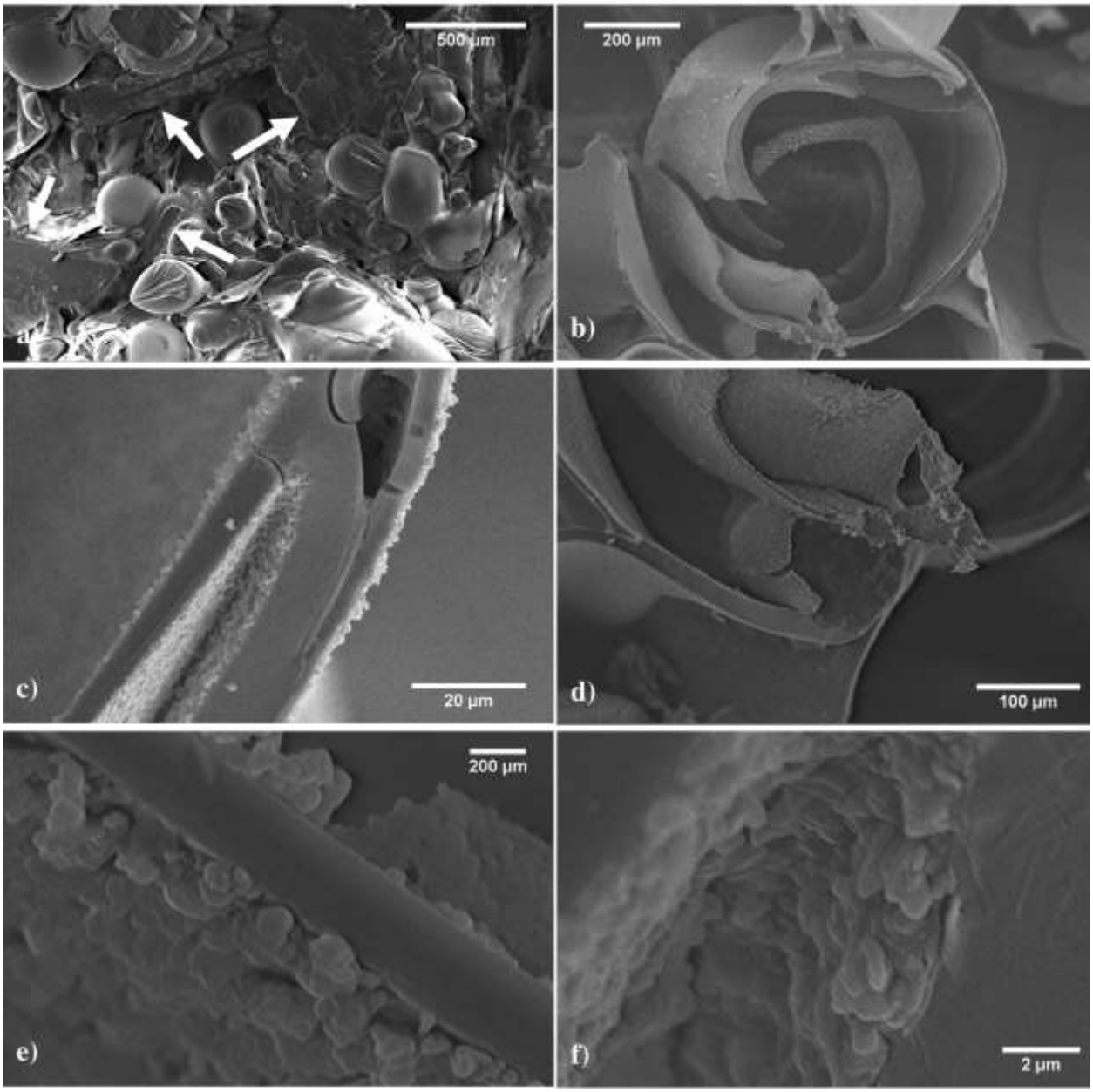

Figure 1. Sponge-like gel evolution with temperature: a) bubbles and crystals of the guest phases (trona, white arrows) into the CG gel sponge; b) to f) early stages of heterogeneous quartz crystallization on the inner and outer walls of the bubbles.

In the CG case, the formation of large gaseous bubbles inside the gel matrix brings to the development of huge cavities with respect to the crystal size, as shown in Figure 1 and **Figure 2**.

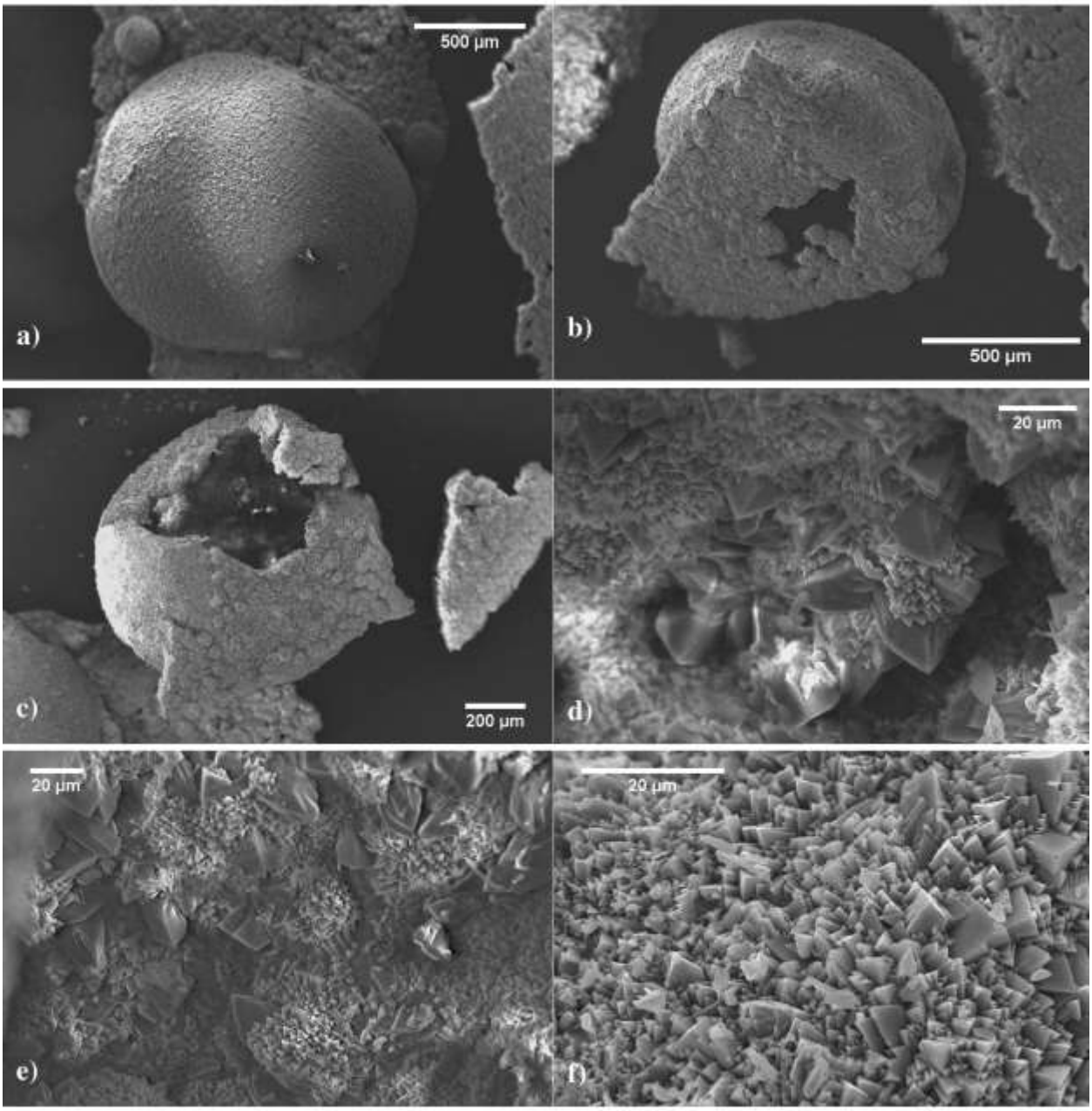

Figure 2. Polycrystalline quartz bubbles grown in CG (a), a polycrystalline quartz bubble detached from substrate (b), the same bubble shown in (b) cracked to highlight the different growth morphology of the inner and outer wall (c), with the inner wall showing a bimodal size distribution of polycrystalline quartz (d and e), and the outer wall showing a more homogeneous crystallization behavior (f).

To verify how the discontinuity induced by bubbles influences the sponge-like behavior of the gel, a growth run was carried out by bubbling N_2 into a NG forming gel. This brought to a clear

morphological convergence in the matrix structures and, as a consequence, on a large scale crystallization behavior very similar to what already observed for CG system (**Figure 3)**. On the contrary, the single crystal morphology and surface quality of the CG and NG+N_2 experiments largely differs. Discrepancies between surface behaviors are maintained because of: i) the chemical surroundings of the crystals, ii) the presence of cooperative growth effects with host phases, and iii) the transport regime imposed by the gel nature, as will be shown in the following section.

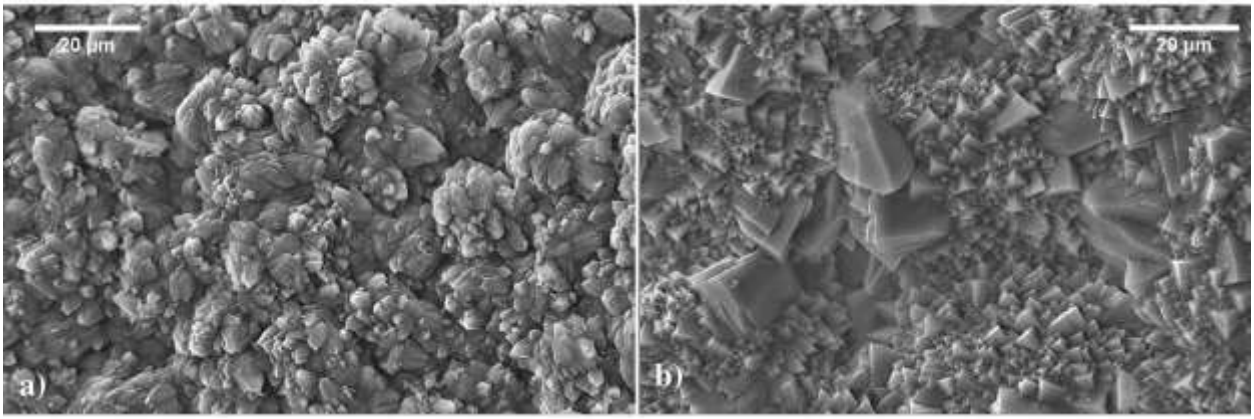

Figure 3. NG with bubbling N_2 during gel formation showing large quartz crystals emerging from the surface of the shell (a); CG gel grown quartz (b).

3.2. Bulk and surface characterization of the synthetic crystals

At the end of the crystallization no foreign phases were detected by XRPD in both NG and CG experiments and α-quartz was the only crystalline phase to be synthetized.

XRPD data were analyzed by the Rietveld method. A comparison between crystal cells and crystallite sizes (see **Figure S1**) was done only on 168 h grown samples, having hypothesized that residual growth should be negligible and, obviously, no more nucleation did occur. Moreover, crystal cells were compared with the NIST SRM 1878a (respirable α-quartz) quartz standard in order to evaluate a cell deformation with respect to a recognized standard. Silicon NIST Standard (SRM 640c) was used to evaluate the instrumental function (**Table 2.**).

The Rietveld refinement shows that the volume of the crystal cell of NG grown quartz is about 0.2% smaller than the CG grown quartz and very similar to the SRM 1878a certified cell ($\Delta <$ 0.03%).

Table 2. Crystal cell parameters (a and c axis length, and cell volume) calculated at room temperature for α-quartz crystals grown in NG and CG gel, respectively. Cell parameters of the NIST SRM 1878a quartz standard are reported for comparison.

	NG grown quartz	SRM 1878a	CG grown quartz
a (Å)	4.9133(3)	4.914	4.9167(4)
c (Å)	5.4050(2)	5.406	5.4083(8)
Cell volume ($Å^3$)	112.9997(3)	113.037	113.2267(2)

At the same time, the averaged crystallite size (evaluated from the refinement data) is 181 nm, for the GC grown crystals, and 119 nm for the NG grown crystals, suggesting, in the first case, a more performing circulation system and a stronger cooperative effect between host phases and quartz, during crystallization.

Particle size distribution (PSD) and specific surface area (BET-SSA) of the synthetic quartz crystals grown in CG and NG for 168 h were evaluated and compared with a natural, high-purity, well characterized α-quartz specimen from Madagascar, milled according to the protocol employed in previous toxicological studies on silica.[31,32] The particle size distribution of the three samples ranges from 100 nm to 2 μm in diameter (**Figure 4**). In the micrometric range, the size distributions of natural and CG quartz are almost superimposable. Some smaller crystals with average diameter of ca. 300 nm are clearly present in the CG grown sample only, resulting in a peculiar bimodal distribution of particle size. The NG synthetic quartz exhibits a much smaller average particle size than CG and natural quartz, with the particle size distribution confined in the sub-micrometric range (100 - 1000 nm). A reduced dispersion index (roughly, the FWHM of the distribution plot) is also observed for NG quartz with respect to CG and natural quartz, that show a more variable range of diameters. The specific surface area of GC and NC

synthetic quartz is 1.1 and 6.2 m^2/g respectively, measured with Kr-BET method. It is worth noting that the natural quartz has a surface area of 6.1 m^2/g, very close to that of NG quartz.

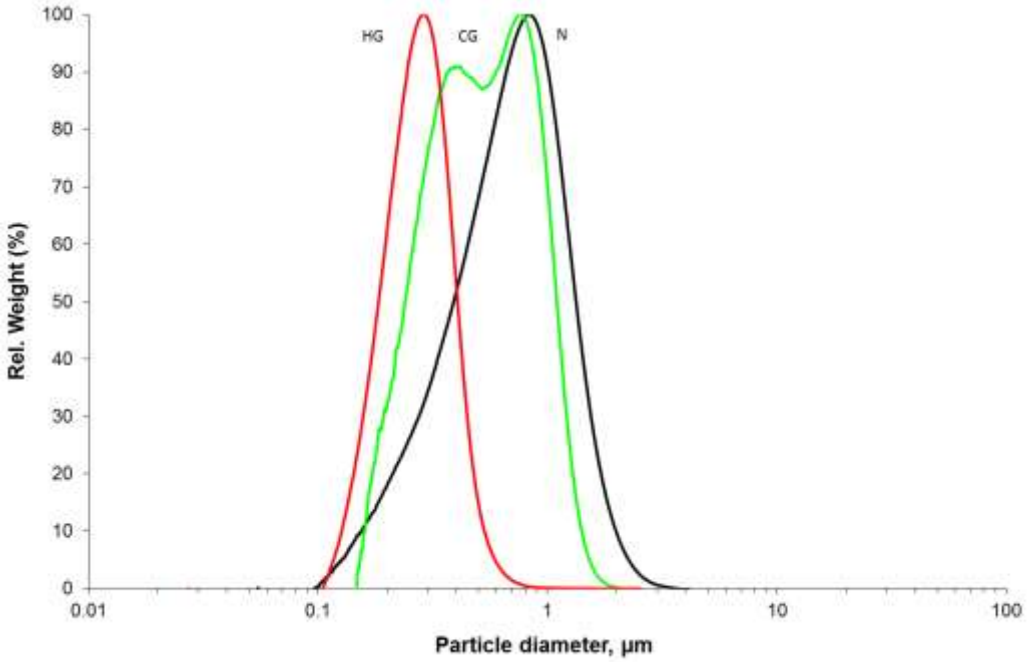

Figure 4. Particle size distribution of CG and NC grown samples (168h), and natural quartz (N). A bimodal size distribution can be observed for CG quartz.

A large body of scientific literature supports the key role of quartz surface chemistry in modulating quartz inflammogenic potential. [8,33,34,35] Quartz surfaces are stabilized by hydrogen bonds between vicinal silanol groups (interacting silanols) and networks of hydrogen bonded silanols are found on all surfaces.[36] Surface silanols (> Si−OH), variously coordinated at the surface, may roughly be described in terms of proximity with other neighboring silanols, Amount and spatial arrangement of silanols affect quartz surface charge and hydrophilic character of quartz, ultimately defining particle behavior toward cell membranes. To characterize the surface chemistry of silica, the chemical proximity of surface silanols is often

evaluated by means of FTIR analysis. The bands in the region between 3800 and 3000 cm^{-1} correspond to the vibrational stretching modes of OH surface groups. A narrow peak at ca. 3750 cm^{-1}, related to the presence of isolated silanols, is commonly reported for both amorphous and crystalline silica [37] and can be observed when physisorbed, hydrogen bonded, water molecules are removed from surface. A broad band in the 3630-3260 cm^{-1} region, associated with different families of interacting silanols, is also observed. In **Figure 5**, the spectra collected on quartz self-supporting pellet in air (a), after outgassing the pellet in vacuum at RT (b), and at 400 °C (c), are reported for NG- and CG-grown quartz, lower and upper series respectively. When molecular water is removed from the surface (spectra b and b'), the narrow peak at 3740 cm^{-1} appears for the NG-, but not for the CG-grown quartz, signaling the occurrence of a family of isolated silanols only on the NG-quartz surface. Further removal of molecular water achieved by heating quartz in vacuum at 400 °C for 45 min (b → c, and b' → c'), does not increase the amount of isolated silanols any further. When thermally outgassed, the CG- and NG-grown quartz show different behaviors. A virtually superimposable spectrum is recorded for NG- (spectra *b* and *c*), while a further loss of molecular water is observed for CG-grown quartz (spectra *b'* and *c'*). This latter feature of CG-grown quartz surface may signal a slightly more hydrophilic behavior with water begin more strongly bound to surface silanols than NG-quartz.

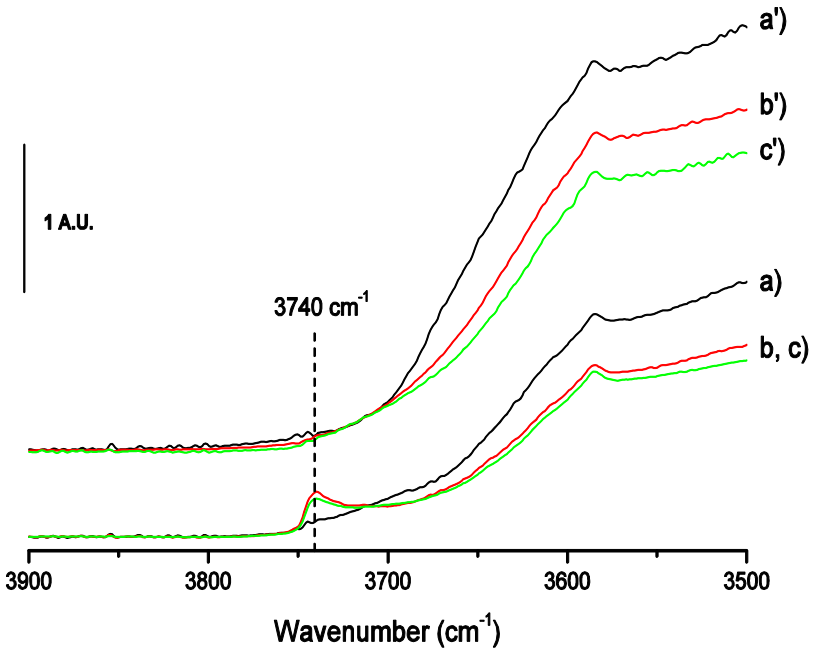

Figure 5. FTIR spectra of the -OH stretching region of NG- and CG-grown quartz collected on self-supporting pellet in air, after outgassing the pellet in vacuum at RT, and at 400 °C (a, b, c, and a', b', c', respectively). No isolated silanols are detected on CG-grown quartz.

3.3. Effect of gel chemistry on the crystal morphology

Concerning the growth morphology, some differences between CG and NG grown crystals may be outlined.

At variance with literature reports about crystallographic {hkil} forms obtained from hydrothermal quartz,[38,39] in all our experiments only one out the two rhombohedra (the direct $\{10\bar{1}1\}$ and the reverse $\{10\bar{1}\bar{1}\}$ one) is always present in the growth morphology, in association with the {1000} prism. No evidences about which one of the two rhombohedra were experimentally obtained.

In CG experiments both rhombohedron and prism forms grow by 3D nuclei juxtaposition. This growth mechanism results in a continuous coverage of a new crystal shell starting from the rhombohedron and overflowing on the prism surface as shown in **Figure 6** b) to f). In Figure 6 d) white arrows evidence the nuclei disposition parallel to the prism striations acting as preferential nucleation sites. At the end of growth, the whole crystal will be encompassed by a growth shell which started from the rhombohedron surface. A similar growth mechanism was already observed by Pastero et al.,[40] when growing anomalous mixed crystal of calcite in the presence of lithium carbonate. An early stage of this process is reported in Figure 6 e) and f) (detail). Here, a macrostep on the cleavage rhombohedron surface is forming, but not yet overflowing onto the prism surface, the coverage being not perfectly uniform.

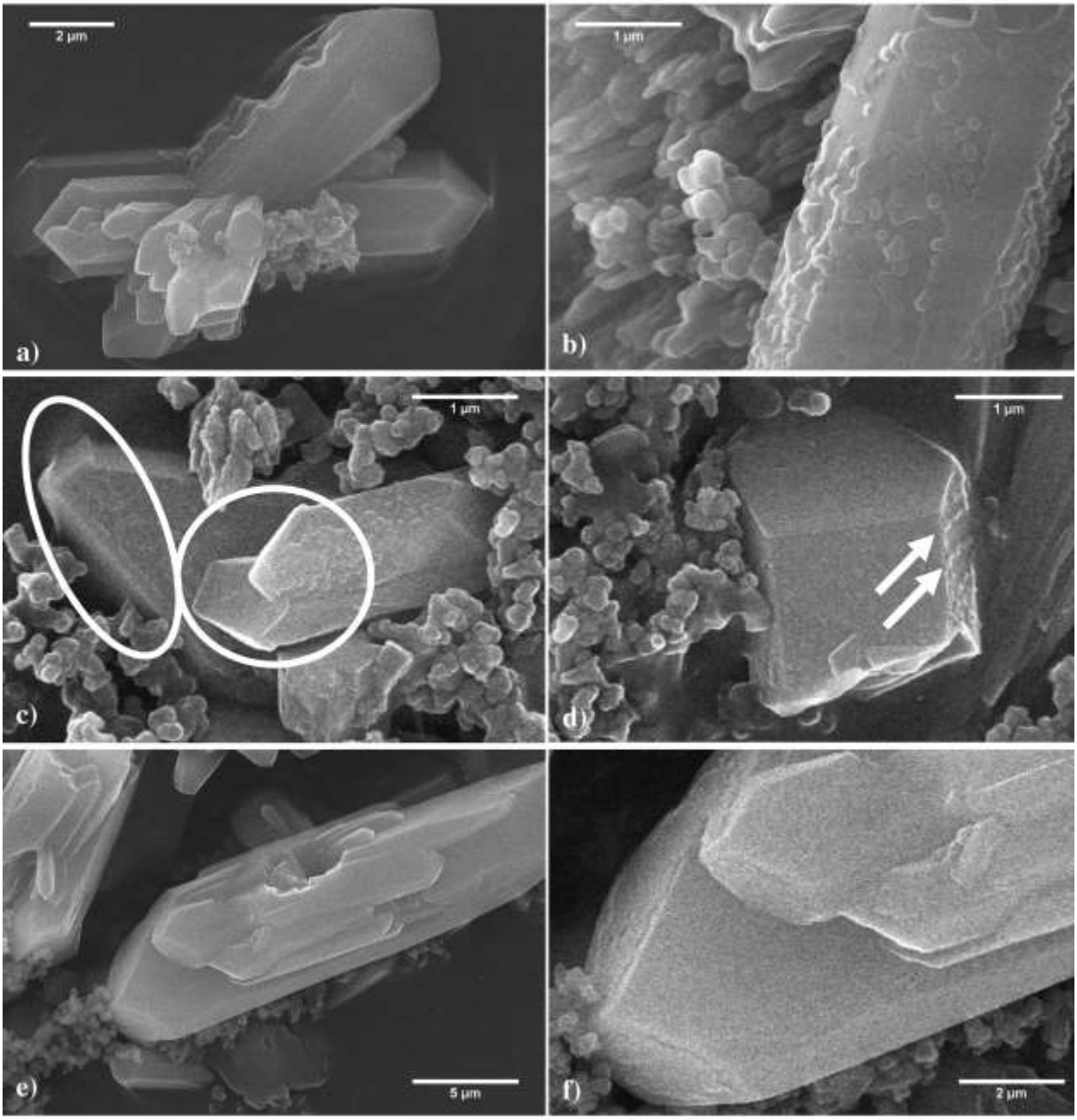

Figure 6. a) CG grown quartz aggregates (SEM pictures), b) 3D nucleation of quartz on prisms surfaces of an older crystal, c) a continuous coverage of a new crystal shell starts from the rhombohedron and overflows on the prism surface, d) nuclei disposition parallel to the prism striations are evidenced by with arrows, e) a CG aggregate and f) a detail of the rhombohedra surfaces

In NG quartz growth, crystals surfaces are smooth and no surface structures are detectable, at low magnification (**Figure 7** a-d). At higher magnification (Figure 7e) a uniformly distributed

rough shell encompassing the whole crystal can be observed. HR-TEM observation (Figure 7f) suggests the occurrence of a few nanometer-thin layer with a lower order degree structure surrounding some well-formed, rounded crystals. In Figure 7c) and d) representative TEM images show that no macrosteps spreading from the rhombohedron to the prism are detectable, as occurred in the CG case.

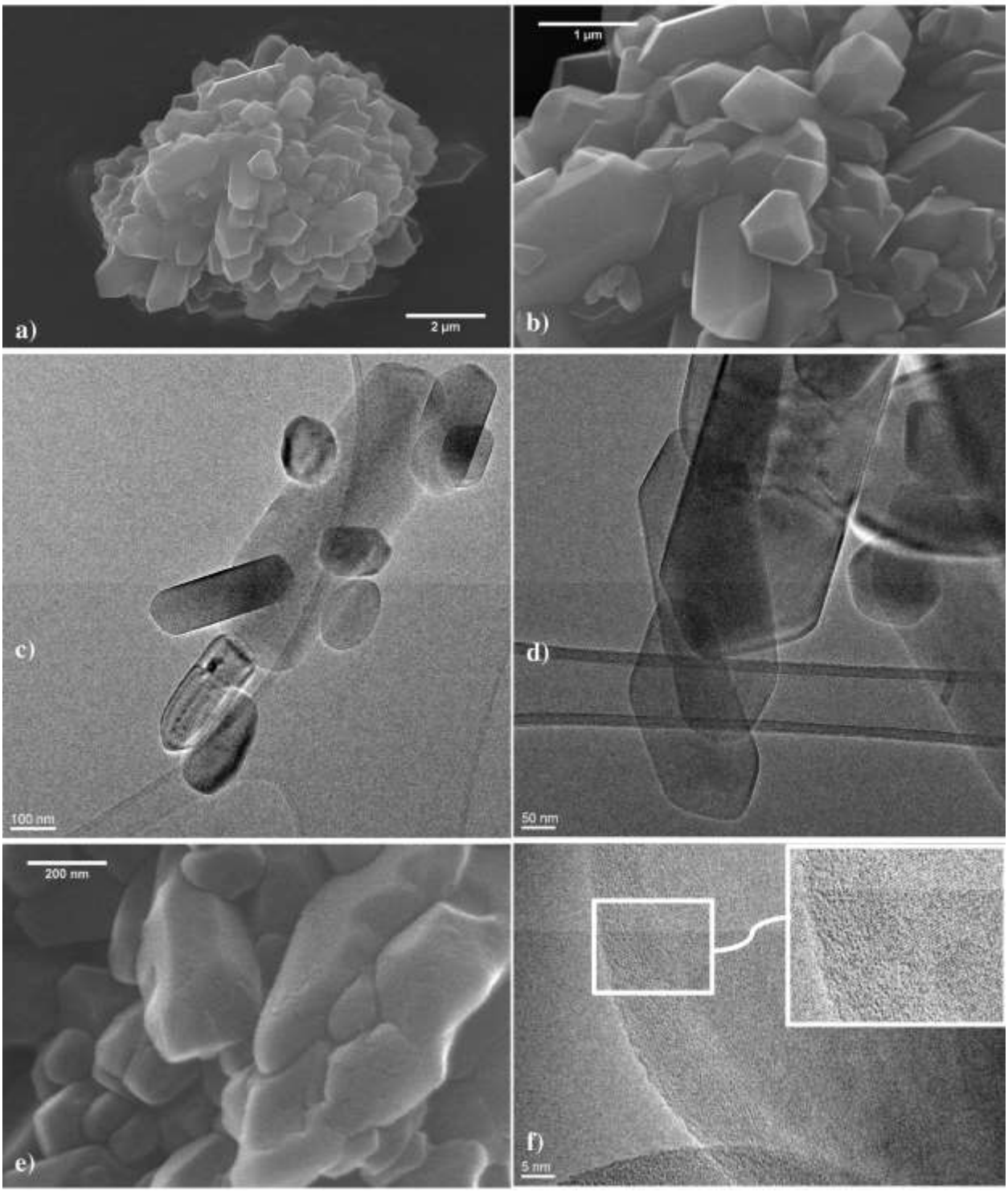

Figure 7. SEM and TEM images of NG as grown aggregates of quartz crystals. a) spherulitic aggregate of NG grown crystals, b) a detail of the previous image, c) and d) TEM image of NG crystals confirming straight edges and very simple morphology, e) NG grown crystals show rough surfaces at SEM high magnification; f) HR-TEM image of the outer shell with the less-ordered structure.

4. Discussion

Keeping in mind that both NG and GC-grown crystals underwent a common thermal treatment, the observed discrepancies in the two quartz samples, namely the crystal morphology and surface behavior, the crystallite size and cell deformation, the specific surface area, and the occurring of different families of silanols at quartz surface, can be ascribed to the chemical and physical differences in the polymerizing agent. In fact HNO_3 is a strong mineral acid and is supplied as solution, while H_2CO_3 is a relatively week diprotic acid and is supplied as CO_2 gas. This induces differences in the two quartz-forming gels that are specifically due to (i) different transport efficiency of the NG- and CG-silica sponges, and (ii) presence of impurities. The supersaturation values locally reached in the two systems cannot be the same because of the different effectiveness in matter transport: at RT only diffusion is virtually present in both gels. At higher temperature a rise in the convective component of transport is observed and that becomes the controlling mechanism for crystal nourishing. The gel role turns from "silica sponge" to silica source and nucleation substrate. In CG, as demonstrated with the gel characterization, convective regime results to be stronger than in NG case, resulting in a more functional medium for crystal growth. The mineral acids used as polymerizing agents during the gel preparation play a fundamental role in determining the chemical surroundings of the quartz crystals. Sodium, present both in CG and NG, is the counter ion in many carbonate phases (also hydrated) and nitrates that could be present. It is well known from literature that the presence of guest phases into the growth environment, even if the solution is unsaturated with respect to the phase, could stabilize new surfaces and/or change their structure.

It is therefore convenient to discuss separately the growth mechanisms of the two quartz-forming gels.

4.1. The CG case

CG polymerization promoted by bubbling CO_2 directly into the NaMTS solution, yields to a more concentrated gel with respect to NG, where NaMTS concentration is lowered by adding HNO_3 aqueous solution. Therefore, even if the absolute content of silica and sodium is the same in both CG and NG cases, the CG system reaches higher supersaturation values with respect to those reached by the NG gel. Furthermore, CO_2 bubbling generates bubbles into the forming gel and a high macro-porosity of the gel is achieved. Rising the temperature during crystallization promotes migration and coalescence of CO_2 bubbles that form large cavities into the gel and act as communicating vessels. The walls of the cavities work as excellent substrates for the heterogeneous nucleation of quartz, lowering the energy amount necessary for the homogeneous nucleation in solution. The silica-rich solution can circulate into the gel cavities and supersaturation value suitable to grow large and well-finished crystals can be preserved throughout the synthesis. Rising the temperature, the gel surrounding the cavities becomes a moving SiO_2 reservoir, as suggested by the compositional data of the flowing solution. Additionally, the presence of free silica is guaranteed by the basic pH values. Bubbles work as heterogeneous nucleation sites and show a double crystallization direction:

i) On the outer bubble wall, the almost constant supersaturation value due to the presence of a semi–infinite reservoir of silica feeding the moving solution, determine the formation of a homogeneous small-sized population of quartz crystals.

ii) On the inner wall the fluid circulation is negligible, silica refill from the surrounding reservoir being impaired. These conditions determine the quartz nucleation to occur under a decreasing supersaturation regime and hence fewer and larger crystals are grown.

The two complementary growth mechanisms are likely the cause of the bimodal size distribution of crystals evidenced by the particle size distribution (PSD) analysis (Figure 4) for CG quartz only.

The higher supersaturation conditions of the CG case are pointed out not only by elemental analysis of the flowing solution (Table 1), but also by the presence of 3D nuclei on the quartz surfaces (Figure 6b-f). It is not surprising that at the end of the experiment, when the temperature rapidly decreases, a shell of small 3D coalescent quartz crystals nucleate on the rhombohedron surfaces forming macrosteps overflowing toward the surfaces of the prisms (Figure 6b-f). Moreover, discussing the overlapping growth process (from the rhombohedron toward the prism), is not trivial. The structure of the crystal surfaces, already described in terms of periodic bond chains (PBC) profiles by Hartman [41] should be put in relationship with the host phases present into the growth medium. From XRPD analysis, trona ($Na_3H(CO_3)_2 \cdot 2H_2O$) as crystalline impurity was detected in CG samples, but all the possible sodium and sodium hydrogen carbonates at different hydration degrees can be encountered during the experiment, depending on the local temperature, pH and composition of the system. At the same time, a large amount of silica and sodium silicate phases at variable hydration levels can occur. Under these conditions, a cooperative effect during growth is expected. It is important to remember that a mechanism of silica gel ordering was already found by Bittarello and coworkers [42] during the growth of silica biomorphs in the presence of whiterite.

The detailed description of the cooperative effects on quartz growth in the presence of all the possible phases coming from the gel speciation is beyond our present purposes and will be discussed in a forthcoming paper.

It is well known from the literature [17,43, 44, 45,46] that the best results on hydrothermal quartz crystal growth are obtained from silica solutions charged with alkali halides and hydroxides as mineralizers. The role of these mineralizers is not only to improve the solubility of silica changing the pH or the quartz solubility according to the ionic strength of the growing bath, but also to cooperate with the growing crystal by acting on its surface structures.

As a matter of fact, one can easily find a very good parametric agreement between the 2D cells of the experimentally obtained forms of quartz and the most frequent forms shown by natural trona crystals, as reported in **Table 3**.

Table 3. Parametric coincidences between quartz (0100 prism and 10-1-1 rhombohedron) and most common growth forms of trona.

Quartz lattice plane	Trona lattice plane	Parametric misfit %
01.0	**001**	
4x[010]=19.6512	[100]=20.36	3.6
2x[001]=10.8084	3x[010]=10.44	3.5
	100	
2x[010]=9.8256	[001]=10.29	4.7
2x[001]=10.8084	3x[010]=10.44	3.5
	010	
2x[010]=9.8256	[011]cosβ=9.8673	0.4
4x[001]=21.6168	[100]=20.36	6.1
10.-1	**001**	
4x[010]=19.6512	[100]=20.36	3.6
[211]=10.0803	3x[010]=10.44	3.5
	100	
2x[010]=9.8256	[001]=10.29	4.7
[211]=10.0803	3x[010]=10.44	3.5
	010	
2x[010]=9.8256	[011]cosβ=9.8673	0.4
2x[211]=20.1606	[100]=20.36	0.9

The 2D parametric coincidences and sharing of PBCs between different crystal species induce a lowering of the surface free energy of both host and guest phases, favoring crystal growth and face smoothness both at atomistic and microscopic level. The lack of isolated silanol (Si-OH) species on the surface of GC quartz, evidenced by FTIR spectroscopy (Figure 5) clearly signals a high uniformity of the surface. In fact, the lack of surface hydroxyl groups not hydrogen bonded

to neighbor (isolated) may likely be related to the large local extension of the 2D spatial order of the CG-grown quartz surface. Isolated silanols on unaltered (e.g., not thermally dehydroxylated) crystalline surface occur preferentially on defective sites, where a limited number of nearest neighbors is available.

The hosting phases epitaxial enhancement on the growth of the GC quartz is further supported by a comparative analysis of specific surface area and particle size measurements. In fact, particle size distribution (Figure 4) indicates that CG quartz crystals are smaller than natural milled quartz. Nonetheless, the surface area is about 6 times smaller. The smoothness of CG-grown crystal faces could possibly explain the very low specific surface area (ca. 1 m^2/g) measured on this sample.

The cooperative effect between hydrated sodium carbonates and quartz is proved also by the quartz crystal cell deformation measured by XRPD and shown in Figure S1.

4.2. The NG case

In the NG case, a slightly higher gel dilution is induced by the water content of the polymerizing agent (aqueous HNO_3). The small amount of air entrapped into the forming gel is negligible if compared with the CG, when CO_2 is forced to enter the solution till the end of gel formation. As a consequence, the bubbles entrapped in the gel become smaller. In this case the bubbles act as nucleation centers, but do not behave as cavities to obtain geode-like growth of quartz crystals. Contrary to what observed inside the large CO_2 bubbles, the lower density and size of bubbles in NG system brings to a more performing gel with truly reduced convection, thus preventing local discontinuities (inside the cavities) in silica supersaturation. Due to their small size, only the outer walls of the bubbles in NG can work as nucleation sites. No lower supersaturation volumes are present in the batch, as happens in CG inner bubbles cavities. Hence, quartz crystals form in the presence of high supersaturation that promotes more nucleation than growth. For this reason,

NG-grown crystals are smaller than CG ones. This explanation is further supported by what observed when NG is forced to become a macro-porous matrix under inert N_2 bubbling. Large bubbles are formed and the uniform arrangement of the silica reservoir falls down, the crystallization behavior becomes, in turn, similar to what observed for CG.

Moreover, in the NG case, the rearrangement of the amorphous polymerized gel toward the ordered phase increasing the temperature seems to be the main quartz growth mechanism, not favored by the cooperative effect of a specific impurity.

In fact, when comparing the structure of the quartz stable surfaces with the surface structure of the most likely hosting phase, i.e. nitratine ($NaNO_3$) a poor parametric agreement between the two phases appears as shown in **Table 4.** In this case, a cooperative mechanism on quartz crystal growth is unlikely.

The rough surfaces evidenced by high-magnification SEM images (Figure 7) and the presence of a thin shell of a phase with a lower ordered lattice structure covering the NG quartz crystal evidenced by HR-TEM analysis (Figure 7f) support this hypothesis. This is a low range rearrangement effect due to the growing crystal surfaces that impose their ordering to the surrounding amorphous phase. The lower crystal cell deformation calculated from Rietveld crystal cell refinements (Figure S1) in this samples supports this hypothesis as well.

Table 4. Parametric coincidences between quartz prism and rhombohedron, and nitratine cleavage rhombohedron.

Quartz lattice plane	Nitratine lattice plane	Parametric misfit %
10.-1	**10.4**	
[100]=4.9128	[010]=5.070	3.2
2x[211]=20.1606	[42-1]=24.318	20.6
01.0	**10.4**	
[010]=4.9128	[010]=5.070	3.2
5x[001]=27.021	[42-1]=24.318	11.1

5. Conclusions

An unusual, easy to perform, and clean synthetic route to obtain a large population of quartz crystals (in the range of nano-micro size) is proposed and discussed. To keep the chemical complexity of the system as low as possible, hydrothermal growth of quartz in mild (T, p) conditions was carried out starting from silica gel polymerized using H_2CO_3 and HNO_3 (CG and NG growth gel, respectively). Quartz grows quickly at low temperature thanks to the presence of nucleation centers (bubbles) which shifts nucleation from homogeneous to heterogeneous, requiring lower activation energy. Moreover, in the CG case, the presence of large bubbles acting as growth cavities with reduced matter transport right inside, locally lowers the supersaturation, moving the process from nucleation to growth. The quality of crystals and surfaces depends on the existence of a cooperation effect between quartz and guest phases during crystal growth, as already proposed in previous works. [40,47]. Guest phases (even if present in solution at concentration lower than the saturation) act as specific surface impurities during growth, lowering the involved surface energies.

The envisaged possibility to fine-tune some key physico-chemical features relevant to quartz toxicity makes this synthetic approach a novel and unique tool for an improved understanding of the molecular mechanisms of the detrimental effect of crystalline silica on human health. A companion paper that specifically addresses this issue has been submitted (Turci et al., submitted).

Supporting Information Available: Figure S1. Comparison between the cell parameters and between cell volume and crystallite size of NG and CG crystals, as calculated by Rietveld refinement.

This material is available free of charge via the Internet at http://pubs.acs.org

Acknowledgements

LP and FT contributed equally to this work. FT (grant UCD-TAF 14) and CP (grant UCD-TAF-122) gratefully acknowledge funding from the European Commission under FP7 Capacities Programme, QualityNano Research Infrastructure (Grant Agreement No: 262163). LP wish to thank Prof. Dino Aquilano for stimulating discussions throughout all the work.

(1) Carretero-Genevrier, A.; Gich, M.; Picas, L.; Gazquez, J.; Drisko, G. L.; Boissiere, C.; Grosso, D.; Rodriguez-Carvajal, J.; Sanchez, C. *Science* **2013**, *340* (6134), 827–831.
(2) Jiang, X.; Bao, L.; Cheng, Y.-S.; Dunphy, D. R.; Li, X.; Brinker, C. J. *Chem. Commun.* **2012**, *48* (9), 1293–1295.
(3) Brinker, C. J. *Journal of Non-Crystalline Solids*. 1988, pp 31–50.
(4) Warheit, D. B.; Webb, T. R.; Colvin, V. L.; Reed, K. L.; Sayes, C. M. *Toxicol. Sci.* **2007**, *95* (1), 270–280.
(5) Rimola, A.; Tosoni, S.; Sodupe, M.; Ugliengo, P. *Chemphyschem* **2006**, *7*, 157–163.
(6) Rabolli, V.; Thomassen, L. C. J.; Princen, C.; Napierska, D.; Gonzalez, L.; Kirsch-Volders, M.; Hoet, P. H.; Huaux, F.; Kirschhock, C. E. A.; Martens, J. A.; Lison, D. *Nanotoxicology* **2010**, *4* (3), 307–318.
(7) Donaldson, K.; Borm, P. J. A. *Ann. Occup. Hyg.* **1998**, *42* (5), 287–294.
(8) Fubini, B. *Ann. Occup. Hyg.* **1998**, *42* (8), 521–530.
(9) Pavan, C.; Rabolli, V.; Tomatis, M.; Fubini, B.; Lison, D. *Part. Fibre Toxicol.* **2014**, *11* (1), 76.
(10) van Berlo, D.; Knaapen, A. M.; van Schooten, F.-J.; Schins, R. P.; Albrecht, C. *Part. Fibre Toxicol.* **2010**, *7* (1), 13.
(11) Mossman, B. T.; Glenn, R. E. *Crit. Rev. Toxicol.* **2013**, *43* (8), 632–660.
(12) *A Review of Human Carcinogens. C. Metals, Arsenic, Fibres and Dusts* -; 2012.
(13) Monopoli, M. P.; Walczyk, D.; Campbell, A.; Elia, G.; Lynch, I.; Bombelli, F. B.; Dawson, K. a. *J. Am. Chem. Soc.* **2011**, *133* (8), 2525–2534.
(14) Napierska, D.; Thomassen, L. C. J.; Rabolli, V.; Lison, D.; Gonzalez, L.; Kirsch-Volders, M.; Martens, J. A.; Hoet, P. H. *Small* **2009**, *5* (7), 846–853.
(15) Napierska, D.; Thomassen, L. C. J.; Lison, D.; Martens, J. a; Hoet, P. H. *Part. Fibre Toxicol.* **2010**, *7* (1), 39.
(16) Ariano, P.; Zamburlin, P.; Gilardino, A.; Mortera, R.; Onida, B.; Tomatis, M.; Ghiazza, M.; Fubini, B.; Lovisolo, D. *Small* **2011**, *7* (6), 766–774.
(17) Bertone, J. F.; Cizeron, J.; Wahi, R. K.; Bosworth, J. K.; Colvin, V. L. *Nano Lett.* **2003**, *3* (5), 655–659.
(18) Li, Li-Jun; Fang, Jiann-Neng; Lo, Huann-Jih; Song, Sheng-Rong; Chen, Yaw-Lin; Chen, Huei-Fen; Lin, I.-C. *J. Chinese Chem. Soc.* **2003**, *50*, 395–398.

(19) Zhdanov, S. P. *ACS Adv. Chem. Ser.* **1971**, *101*, 20–43.
(20) Prieto, M.; García-Ruiz, J. M.; Amorós, J. L. *J. Cryst. Growth* **1981**, *52*, 864–867.
(21) McCauley, J. W.; Roy, R. *Am. Mineral.* **1974**, *59*, 947–963.
(22) Pastero, L.; Costa, E.; Alessandria, B.; Rubbo, M.; Aquilano, D. *Journal of Crystal Growth*. January 2003, pp 472–482.
(23) Garcia-Ruíz, J. M.; Gonzalez-Ramirez, L. A.; Gavira, J. A.; Otálora, F. *Acta Crystallogr. Sect. D Biol. Crystallogr.* **2002**, *58* (10), 1638–1642.
(24) Moran, P. A. P. *The Theory of Storage*; Methuen: London, 1959.
(25) Cetini, G.; Ricca, F. *Ric. Sci.* **1960**, *7*, 994–1009.
(26) Kirov, G. K.; Vesselinov, I.; Cherneva, Z. *Krist. und Tech.* **1972**, *7* (5), 497–509.
(27) Kirov, G. K. In *Growth of Crystals,Vol.12*; Chernov, A. A., Ed.; Springer: Berlin, 1984; p 355.
(28) Parkhurst, D. L.; Appelo, C. A. J. In *U.S. Geological Survey Techniques and Methods, Book 6*; USGS, 2013; p 497.
(29) Lutterotti, L.; Bortolotti, M.; Ischia, G.; Lonardelli, I.; Wenk, H.-R. *Zeitschrift für Krist. Suppl.* **2007**, *2007* (suppl_26), 125–130.
(30) Lutterotti, L. *Nucl. Instruments Methods Phys. Res. Sect. B Beam Interact. with Mater. Atoms* **2010**, *268* (3-4), 334–340.
(31) Ghiazza, M.; Polimeni, M.; Fenoglio, I.; Gazzano, E.; Ghigo, D.; Fubini, B. *Chem. Res. Toxicol.* **2010**, *23* (3), 620–629.
(32) Pavan, C.; Tomatis, M.; Ghiazza, M.; Rabolli, V.; Bolis, V.; Lison, D.; Fubini, B. *Chem. Res. Toxicol.* **2013**, *26* (8), 1188–1198.
(33) Donaldson, K.; Stone, V.; Duffin, R.; Clouter, A.; Schins, R.; Borm, P. *J. Environ. Pathol. Toxicol. Oncol.* **2001**, *20 Suppl 1*, 109–118.
(34) Ghiazza, M.; Scherbart, A. M.; Fenoglio, I.; Grendene, F.; Turci, F.; Martra, G.; Albrecht, C.; Schins, R. P. F.; Fubini, B. *Chem. Res. Toxicol.* **2011**, *24* (1), 99–110.
(35) Peeters, P. M.; Eurlings, I. M. J.; Perkins, T. N.; Wouters, E. F.; Schins, R. P. F.; Borm, P. J. A.; Drommer, W.; Reynaert, N. L.; Albrecht, C. *Part. Fibre Toxicol.* **2014**, *11* (1), 58.
(36) Murashov, V. V. *J. Phys. Chem. B* **2005**, *109* (9), 4144–4151.
(37) Zhdanov, S. P.; Kosheleva, L. S.; Titova, T. I. *Langmuir* **1987**, *3* (6), 960–967.
(38) Friedel, C.; Sarrasin, E. *Bull. la Société Minéralogique Fr.* **1879**, *4*, 113–117.
(39) de Kroustchoff, M. K. *C. R. Hebd. Seances Acad. Sci.* **1887**.
(40) Pastero, L.; Aquilano, D. *Cryst. Growth Des.* **2008**, *8* (9), 3451–3460.
(41) Hartman, P. *Bull. la Société française Minéralogie* **1959**, *82*, 335–340.
(42) Bittarello, E.; Massaro, F. R.; Rubbo, M.; Costa, E.; Aquilano, D. *Cryst. Growth Des.* **2009**, *9* (2), 971–977.
(43) Jiang, X.; Jiang, Y.-B.; Brinker, C. J. *Chem. Commun. (Camb).* **2011**, *47* (26), 7524–7526.
(44) Swinnerton, A. C.; Owen, G. E.; Corwin, J. F. *Discuss. Faraday Soc.* **1949**, *5*, 172.
(45) Wooster, N.; Wooster, W. A. *Nature* **1946**, 297.
(46) Brown, C. S.; Kell, R. C. .; Thomas, L. A.; Wooster, N.; Wooster, W. A. *Nature* **1951**, *167*, 940–941.
(47) Aquilano, D.; Pastero, L. *Cryst. Res. Technol.* **2013**, *48* (10), 819–839.

For Table of Contents Use Only

Synthesis of α-Quartz with Controlled Properties for the Investigation of the Molecular Determinants in Silica Toxicology

Linda Pastero, Francesco Turci, Riccardo Leinardi, Cristina Pavan, Marco Monopoli

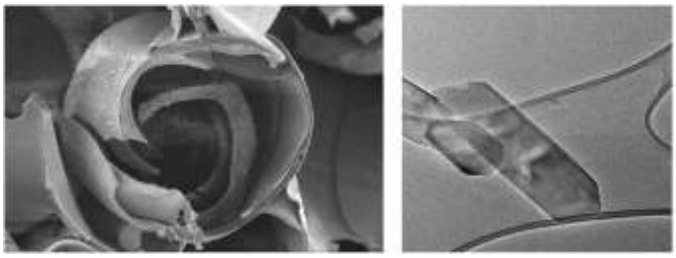

The carcinogenic effects of the crystalline silica are well recognized. The relationship between surface structure and toxicological effects is not yet well understood. Alpha-quartz crystals with controlled properties are synthesized under mild hydrothermal conditions following a brand new, smart and clean synthesis routine. The crystal growth mechanisms involved are described and discussed.